Applied Surface Science 598 (2022) 153849

Contents lists available at ScienceDirect

Applied Surface Science

journal homepage: www.elsevier.com/locate/apsusc

Full Length Article

In-situ growth of MnO_2 on hierarchical porous carbon foam with enhanced oxygen vacancy concentration and charge transfer for efficient catalytic oxidation of 5-hydroxymethylfurfural

Min Jiang, Furui Hu, Guifen Feng, Hongguang Zhang, Huayu Hu *, Tao Gan, Zuqiang Huang, Yanjuan Zhang *

School of Chemistry and Chemical Engineering, Guangxi University, Nanning 530004, China

ARTICLE INFO

Keywords:
Catalytic oxidation
5-Hydroxymethylfurfural
2,5-Furanediformic acid
MnO_2
Carbon foam

ABSTRACT

The catalytic oxidation of biomass-derived 5-hydroxymethylfurfural (HMF) to prepare 2,5-furandicarboxylic acid (FDCA) is a promising route to produce biomass-based functional materials. It is significant to develop non-noble metal-based catalysts for efficient conversion of HMF to FDCA. In this study, a facile and green technology was developed to prepare hierarchical porous carbon foam (CF)-supported MnO_2 (MnO_2/CF) catalyst by in-situ growth of MnO_2 nanoparticles on blocky CF, and the catalytic activity of MnO_2/CF for the oxidation of HMF to FDCA was evaluated. Under mild reaction conditions, the MnO_2/CF catalyst achieved 99.8% conversion of HMF and 97.0% yield of FDCA, which was well beyond the catalytic performance of single MnO_2. The results indicated that the CF with hierarchical porous structure and oxygen-containing groups could facilitate the diffusion of reactant molecules and regulate the crystal structure and morphology of MnO_2. The synergistic interaction of CF and MnO_2 effectively enhanced specific surface area, surface acid-base sites, oxygen vacancy concentration, and charge transfer efficiency of MnO_2/CF composite, contributing to favorable catalytic performance. Additionally, the MnO_2/CF catalyst showed promising stability and reusability. This work provides new insights into the development of efficient, stable, and economical non-noble metal-based catalysts for catalytic conversion of biomass-based chemicals.

1. Introduction

With the rapid depletion of non-renewable fossil resources (oil, coal, natural gas, etc.) and the increasing emission of greenhouse gases, the development of renewable resources is attracting more and more attention. Abundant and low-cost renewable biomass is a promising alternative for the sustainable production of important chemicals and fuels for our society [1–3]. As one of the biomass-based key platform chemicals, 5-hydroxymethylfurfural (HMF) is a versatile intermediate for the production of value-added fine chemicals and liquid fuels by selective hydrogenation or oxidation [4–7]. 2,5-furan dicarboxylic acid (FDCA) derived from the selective oxidation of HMF has cyclic structure and di-acidic side chains, which can be regarded as an important monomer. Especially, the polymerization of FDCA and ethylene glycol can produce polyethylene furandicarboxylate (PEF), which has gained significant popularity as a potential replacement to petroleum-based poly(ethylene terephthalate) (PET) [8,9]. Therefore, efficient catalytic oxidation of HMF to FDCA is of great significance for sustainable development of biomass-based functional materials.

As reported in numerous literatures, the production of FDCA was usually performed under harsh reaction conditions [10,11]. The efforts on developing efficient catalytic systems under mild conditions mainly focused on noble metal-based catalysts, which exhibit excellent activity on the catalytic conversion of HMF into FDCA because of the special d track structure. However, the high cost and scarcity of precious metals restrict their wide application in industry [12–16]. Consequently, it is still a challenge to develop non-noble metal-based catalysts with performance comparable to that of noble metal-based catalysts. Manganese has received extensive attention in the catalytic oxidation of HMF to FDCA due to its excellent redox properties, multivalent chemical properties, and economical advantages of low cost [17–23]. Liu et al. [24] proposed a simple and green vitamin C-assisted solid-phase milling method to prepare Mn-Co spinel oxides with enhanced oxygen vacancy (O_v) concentration. The yield of FDCA offered 96% under the conditions

* Corresponding authors.
E-mail addresses: yuhuahu@163.com (H. Hu), zhangyj@gxu.edu.cn (Y. Zhang).

https://doi.org/10.1016/j.apsusc.2022.153849
Received 26 March 2022; Received in revised form 17 May 2022; Accepted 28 May 2022
Available online 31 May 2022
0169-4332/

of 130 °C, 1.5 MPa air, and 3 h, demonstrating the feasibility and excellence of manganese-based catalysts in HMF oxidation reaction. Zhou et al. [25] reported that isotopic labeling experiments revealed that molecular oxygen acted as an electron scavenger in the conversion of HMF to FDCA and formed reactive oxygen species, which could remove protons from hydrogen-metal intermediates and recover catalysts. Thus, efficient catalysts for the aerobic oxidation of HMF need not only fast and reversible redox performance, but also strong substrate and oxygen adsorption activation ability. Wei et al. [26] demonstrated that O_v on the catalyst surface could promote the activation of O_2 to form reactive oxygen species and accelerate the transfer of hydrides during the oxidation of alcohol groups. Based on this phenomenon, the catalyst should be designed to form more lattice defects to obtain higher O_v concentration. It is generally accepted that the acid-base properties of catalysts have a great influence on the catalytic performance. The acidic sites of the catalyst are conducive to the adsorption of the aldehyde groups of HMF on the surface of catalyst, while the basic sites can further convert it into the intermediate hemiacetal and accelerate its deprotonation [12,27,28]. In fact, α-MnO_2 has been proven to have unique chemisorption properties and a small charge transfer resistance [29,30]. Unfortunately, there are few O_v amount and Lewis acid-base pairs sites on the surface of α-MnO_2, so it is easy to be ignored in the application of catalytic oxidation of HMF. In addition, manganese-based catalysts are mainly powdery or granular, which are difficult to recover and exhibit low stability [31,32].

Currently, metal oxides are commonly chosen as supports, but they are prone to sintering or structural collapse in reaction system; MOF materials with high cost and complex preparation process are not economically feasible; activated carbons with small pore size are not conducive to the diffusion of reactants and products. Moreover, most of these support materials are also powdery. The blocky supported catalysts manifest great advantages in the stability, reusability, and processability. However, there are few studies on blocky manganese-based catalysts, which may be ascribed to the lack of green, low-cost, and facile methods for the fabrication of blocky support materials and in-situ growth of manganese-based active components on support. In this light, the rational design of blocky support materials can promote the catalytic performance and commercialization of manganese-based catalysts in the application of HMF oxidation.

Carbon foam (CF) is a new functional carbon material with low density, good thermal stability, high corrosion resistance, impact resistance, and high electrical conductivity. The CF with these unique advantages can be used as an excellent support material for nanocatalysts. Wang et al. [33] adopted CF as hard-template and PVP as soft-template to control the growth of BiOBr, and flower-like BiOBr/CF/PVP composite catalysts were synthesized for photocatalytic degradation of rhodamine B. Hopefully, the use of CF as the support for preparing blocky non-noble metal-based catalysts can effectively promote the performance for catalytic oxidation of HMF to FDCA. The three-dimensional (3D) skeleton of CF not merely acts as a support but can also improve the mass transfer process of the reaction and provide sufficient specific surface area for the adsorption of substrates and oxygen, thus enhancing the adsorption capacity and electron transport capacity of the blocky catalyst.

Herein, to overcome the disadvantages of powdery manganese-based catalysts in practical applications, hierarchical porous CF with high-strength and 3D interconnected structure was fabricated by incomplete carbonization of nitrogen-containing precursor, which was used as the support material of MnO_2 nanoparticles to prepare MnO_2/CF composite for catalytic oxidation of HMF to FDCA. Owing to rich functional groups of CF, Mn ions could anchor on the surface of CF for in-situ growth of MnO_2 to form stable blocky MnO_2/CF composite. The key roles of CF in regulating the structure and surface properties of MnO_2 and enhancing the catalytic activity of the catalyst were explored by comparative investigation of the structural characteristics, electrochemical properties, adsorption capacity, and catalytic performance of MnO_2/CF and MnO_2. Especially, the effects of O_v concentration and charge transfer efficiency on the catalytic activity of the catalyst were evaluated. Furthermore, the recyclability was studied to verify the structural stability of the catalyst, and the possible reaction mechanism for the catalytic oxidation of HMF to FDCA over MnO_2/CF catalyst was also proposed. This study can provide a promising strategy to develop economic non-noble metal-based catalysts for efficient conversion of HMF to FDCA.

2. Materials and methods

2.1. Materials

All reagents were obtained from commercial sources and used directly without purification. HMF (99%), FDCA (98%), 5-hydroxymethyl-2-furancarboxylic acid (98%, HMFCA), 2,5-furan-dicarbaldehyde (DFF, 98%), and 5-formyl-2-furancarboxylic acid (FFCA, 98%) were obtained from Shanghai Aladdin Biochemical Technology Co., Ltd. China. Cassava starch was supplied by Guangxi State Farms Mingyang Starch Development Co., Ltd. (Nanning, China). Gluten protein (9.6% moisture, 85.8% protein content in the dry basis) was purchased from Henan Lotus Flour Co., Ltd. (Xiangcheng, China). Instant dry yeast powder (Angel, China) was purchased from a local supermarket. Nitric acid (65–68 wt%, HNO_3) was obtained Chengdu Cologne Chemicals Co., Ltd., China. $KMnO_4$ (>99%), $MnSO_4·H_2O$ (>99%), and $NaHCO_3$ (>99%) were purchased from Sinopharm Chemical Reagent Co., Ltd. (Guangzhou, China).

2.2. Catalyst preparation

2.2.1. Preparation and pretreatment of CF

CF was prepared according to the method described in our previous work [34]. Typically, 30 g of cassava starch and 9 g of gluten protein were put into a ball mill with the addition of 300 mL of zirconia milling balls. After milled for 10 min at a speed of 300 rpm, the damaged starch and gluten protein were separated from the milling balls by a sieve. The dried yeast powder (0.2 g) was dissolved in deionized water (10 mL), and then 10 g of the damaged starch and gluten protein was added and the mixture was evenly mixed by stirring. The mixture was kneaded into a smooth dough, which was fermented for 1 h in an incubator at a constant temperature of 40 °C and relative humidity of 90%. The fermented dough was steamed in a pot for 20 min to prepare porous bread, and then was dried at 150 °C for 5 h. The dry porous bread was calcined in a tube furnace under N_2 at 500 °C for 2 h. After natural cooling to room temperature, the resulting CF was obtained to cut it into small pieces with a size of approximately 3 mm × 3 mm × 3 mm. Subsequently, CF (2 g) was added in 40 mL of HNO_3 solution (1 M) and refluxed at 90 °C for 1.5 h to prepare acidified CF.

2.2.2. Preparation of MnO_2/CF

A certain amount of $MnSO_4·H_2O$ was dissolved in 10 mL of deionized water by vigorous stirring to obtain solution A; A certain amount of $KMnO_4$ was dissolved in 20 mL of deionized water by vigorous stirring to obtain solution B. The amount of $MnSO_4·H_2O$ and $KMnO_4$ were added according to the molar ratio of 3:2. The acidified CF (2 g) was added into solution A and stirred continuously to obtain the suspension. Next, solution B was slowly dropped into the suspension. The mixture was stirred for 10 h at 50 °C in a water bath for the in-situ growth of MnO_2 on CF. After the reaction, the solid product was washed several times with deionized water and ethanol, and MnO_2/CF was obtained by drying at 70 °C for 12 h. Moreover, the MnO_2/CF composites with various loading amount of MnO_2 were prepared by varying the Mn^{2+} concentration of (0.36, 0.72, 1.08, 1.44, 1.80, 1.98, and 2.16 M) in the solution. The preparation process of MnO_2/CF is illustrated in Fig. 1.

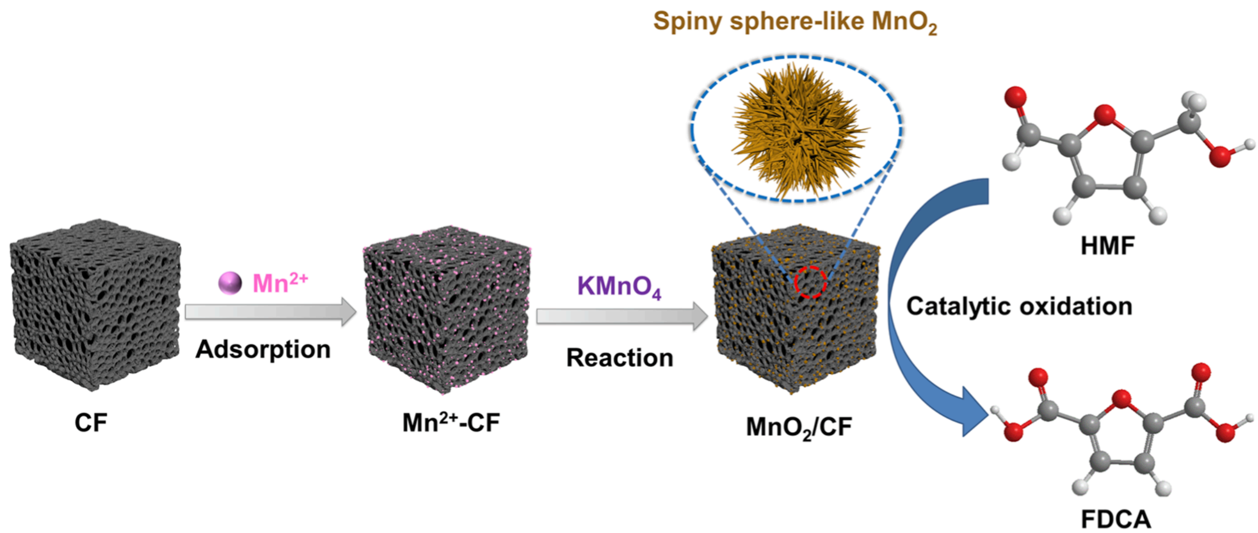

Fig. 1. Schematic diagram of the preparation process of MnO_2/CF catalyst.

2.2.3. Preparation of MnO_2

MnO_2 was obtained by the same preparation method as MnO_2/CF, but without the addition of CF.

2.3. HMF adsorption experiments

The test method refers to the procedure reported in the literature [35]. CF, MnO_2, or MnO_2/CF was added into 5 mL of HMF solution (0.05 M) and stirred at room temperature. After 120 min of adsorption, the solid sample was separated from the solution system by filtration, and the concentration of HMF in solution was quantitatively detected by high performance liquid chromatography. The adsorption capacity (Q_T, mg g^{-1}) of different samples for HMF was calculated by Eq. (1).

$$Q_T = \frac{C_0 - C_e}{m} \times V \tag{1}$$

where C_0 and C_e are initial and equilibrium concentrations of HMF, V is the volume of solution, and m is the weight of different samples.

2.4. Catalytic oxidation of HMF

The catalytic oxidation experiments of HMF were performed in a 25 mL autoclave. Typically, HMF (0.25 mmol), $NaHCO_3$ (0.5 mmol), H_2O (5 mL), and MnO_2/CF catalyst (0.4 g) were added to the autoclave. The autoclave was then purged three times with O_2, and then 0.3 MPa O_2 was charged into the reactor. Subsequently, the reaction was performed at 100 °C for 2 h under constant stirring. After cooling, the liquid product was obtained by filtration to remove the catalyst. The collected catalyst was washed with water and ethanol, and then was dried at 70 °C for 12 h and sealed for reuse.

The liquid product was analyzed by high-performance liquid chromatography (HPLC) system (Thermo UltiMate 3000, USA) equipped with a UV–vis detector and Aminex HPX-87H (300 mm × 7.8 mm) column. The mobile phase of HPLC was 0.005 M H_2SO_4 with a flow rate of 0.6 mL/min, and the column temperature was 60 °C. The external standard method was used for quantitative analysis of the product. The conversion rate of HMF and the yield of FDCA/FFCA were calculated by the following equations. All catalytic reactions were conducted in triplicate to obtain statistical average values.

$$C_{HMF}(\%) = \left(1 - \frac{molofHMFintheproducts}{initialmoleofHMF}\right) \times 100\% \tag{2}$$

$$Y_X(\%) = \frac{molofXintheproducts}{initialmoleofHMF} \times 100\% \mathrm{X} = (\mathrm{FDCA\ or\ FFCA}) \tag{3}$$

2.5. Characterizations

X-ray diffraction (XRD) patterns under Cu Kα radiation were collected using an Ultima IV diffractometer (Rigaku, Japan) to analyze the physical phases and crystal structures of the samples (scanning angle 5°-80°, scanning speed 10° min^{-1}). The specific surface area and pore size distribution of the samples were measured on a NOVA 4200E nitrogen adsorption instrument (Quantachrome, Germany) using the Brunauer-Emmett-Teller (BET) method and the Barrett-Joyner-Halenda (BJH) model, respectively. The surface chemical states and stoichiometric composition of the catalysts were determined by X-ray photoelectron spectroscopy (XPS) on a K-Alpha$^+$ X-ray photoelectron spectrometer (Thermo Fisher Scientific, USA) at monochrome Al Kα radiation (hv = 1486.6 eV). The functional groups of the samples were determined on a Fourier transform infrared (FT-IR) spectrometer on a Nicolet IS50 spectrometer (Thermo Fisher Scientific, USA) using the KBr technique with a resolution of 4 cm^{-1} and a frequency range of 500–4000 cm^{-1}. The morphology of the samples was observed by a Supra55 field emission scanning electron microscopy (FESEM, Carl Zeiss, Germany) at an accelerated voltage of 2.00 kV, and enlarged areas were observed by a Tecnai G2 F30 field emission high-resolution transmission electron microscopy (HRTEM, FEI, USA) at an accelerating voltage of 300 kV. Electron paramagnetic resonance spectroscopy (EPR, Bruker A300, Germany) was used to determine the O_v concentration by measuring the electrons trapped by the O_v. The electrochemical impedance spectra (EIS) were measured on an electrochemical workstation (CHI 760E, China) to investigate the charge transfer resistance of the samples, with platinum electrode as the counter electrode, saturated calomel electrode (SCE) as the reference electrode, glassy carbon electrode (GCE) or sample-modified GCE as the working electrode, and 5 mM $K_3[Fe(CN)_6]/K_4[Fe(CN)_6]$ (1:1) solution as the electrolyte. Temperature-programmed reduction of ammonia and carbon dioxide (NH_3-TPD and CO_2-TPD) measurements were performed using AutoChem II 2920 station equipped with a TCD detector (Micromeritics, USA) to determine the surface acidity and alkalinity of the catalysts. Prior to TPD tests, the sample (0.1 g) was pretreated at 300 °C for 1 h in He flow (99.9%, 120 mL min^{-1}). After cooling to 50 °C, the sample was saturated under 10% NH_3/He (or high-purity CO_2) flow for 30 min, followed by introducing He flow for 1 h to purge physiosorbed NH_3 or CO_2. Finally, the desorption was carried out at a heating rate of 15 °C

min^{-1} to 650 °C under He atmosphere, and the desorbed NH_3 or CO_2 was detected by TCD. The metal content of the samples was determined by inductively coupled plasma atomic emission spectroscopy (ICP-OES, Aglient 5110, USA).

3. Results and discussion

3.1. Preparation and structural analysis of the catalysts

In this study, a facile strategy was developed to prepare MnO_2/CF catalyst by in-situ growth of MnO_2 nanoparticles on 3D hierarchical porous CF. As illustrated in Fig. 1, the oxygen-containing groups on the surface of CF served as anchoring sites to adsorb Mn^{2+} in the outer surface and pore walls to form Mn^{2+} complexes. With the dropwise addition of $KMnO_4$ solution, a large number of spiny sphere-like MnO_2 nanoparticles were formed and deposited on the CF through the process of "complexation-reaction growth" [36]. CF still maintained the 3D pore structure after in-situ growth of MnO_2 because of the special and stable pore structure characteristics, resulting in favorable catalytic activity of MnO_2/CF.

3.1.1. XRD analysis

As shown in Fig. 2a, two wide diffraction peaks at near 24° and 42° in the XRD pattern of CF can be indexed to (0 0 2) and (1 0 0) diffraction planes of graphitized carbon, respectively, confirming a typical amorphous structure [37]. The XRD pattern of the single MnO_2 exhibited the diffraction peaks at 37.2° and 66.0°, but these diffraction peaks were wide and weak, which may be attributed to low crystallinity or small crystal size. By contrast, the XRD pattern of MnO_2/CF revealed perfect characteristic α-MnO_2 diffractions (JCPDS No. 00-044-0141) [38], with stronger intensity of the diffraction peaks and the exposure of more crystal planes. This can be ascribed to that the surface of CF contained a large number of oxygen-containing groups, which could form strong coordination interactions with MnO_2 and had a significant effect on the crystal structure of MnO_2 [36,39]. In addition, the oxygen-containing groups promoted the adsorption of K^+, and the adsorbed K^+ could enter the interior of the MnO_2 crystal and affect the crystal structure [40].

3.1.2. FT-IR spectroscopy

FT-IR was applied to analyze the functional groups of the samples, and the results are shown in Fig. 2b. The infrared spectra of all samples exhibited a strong absorption peak at 3436 cm^{-1}, assigned to the stretching vibration of –OH. The absorption peaks at 1608, 1265, and 1123 cm^{-1} were attributed to the characteristic absorption of oxygen-containing groups. The presence of a large number of oxygen-containing groups on the surface of CF provided anchoring sites for the adsorption of Mn^{2+} and the in-situ growth of MnO_2. The absorption peak at 1380 cm^{-1} corresponded to C–N stretching. The characteristic peaks of MnO_2 at 525 and 716 cm^{-1} arose from the stretching vibrations of Mn–O and Mn–O–Mn bonds. MnO_2/CF showed distinct characteristic peaks at 525 and 716 cm^{-1}, demonstrating that MnO_2 was successfully formed on the CF.

3.1.3. Specific surface area and pore structure analysis

The N_2 adsorption/desorption isotherms and pore size distributions of CF, MnO_2, and MnO_2/CF are displayed in Fig. S1. The BET specific surface area (S_{BET}) of single MnO_2 was 222.8 m^2 g^{-1}, which far exceeds that of most previously reported MnO_2 catalysts [30,41]. CF show a high S_{BET} of 384.2 m^2 g^{-1}, resulting from the formation of hierarchical porous structure. Surprisingly, the combination of CF and MnO_2 apparently improved the S_{BET} of the catalyst, resulting in the highest S_{BET} (430.3 m^2 g^{-1}) of the resultant MnO_2/CF catalyst. This may be attributed to the special pore structure and oxygen-containing groups of CF provided a framework with abundant sites for the formation of the 3D spiny sphere-like MnO_2 with large specific surface area. Therefore, the S_{BET} of MnO_2/CF was higher than that of single MnO_2 and CF. In general, the S_{BET} of support reflects the exposed surface area for supporting catalytic active components, and the increase in the S_{BET} of support is beneficial to the increase of active sites on the surface of the catalyst. The pore structure of the support changes the degree of diffusion of the active sites on the support, and the high S_{BET} makes the substrates and products in the catalyst channels more accessible to the active sites during the diffusion process. CF has a network structure of intertwined and interconnected large and small pores. The macropores improve the mass transfer process of the reaction, and the mesopores and micropores can adsorb oxygen and improve the activation efficiency of oxygen. As shown in the inset in Fig. S1, MnO_2 exhibited a narrow pore size distribution, and CF and MnO_2/CF presented slightly larger pore size distribution, which is beneficial for the diffusion of substrates and products.

3.1.4. Morphological analysis

The morphology and microstructure of different samples are shown in the Fig. 3. FESEM image discloses that CF presents a 3D interconnected porous structure (Fig. 3a), attributed to the fermentation and carbonization procedures in the preparation process of CF. In this structure, the reactants can easily diffuse through the pores into the interior of the solid catalyst and make full contact with the active sites, and the products can diffuse out smoothly through the pore channels, improving the mass transfer process of the catalytic reaction. As can be observed from the FESEM image of MnO_2/CF (Fig. 3b), the MnO_2 nanoparticles were distributed on the outer surface and pore walls of the

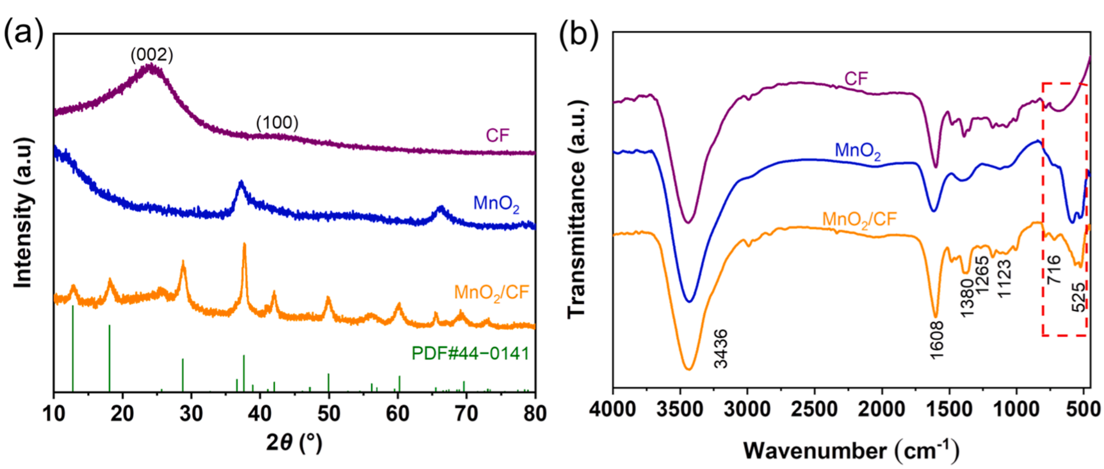

Fig. 2. (a) XRD patterns and (b) FT-IR spectra of CF, MnO_2, and MnO_2/CF.

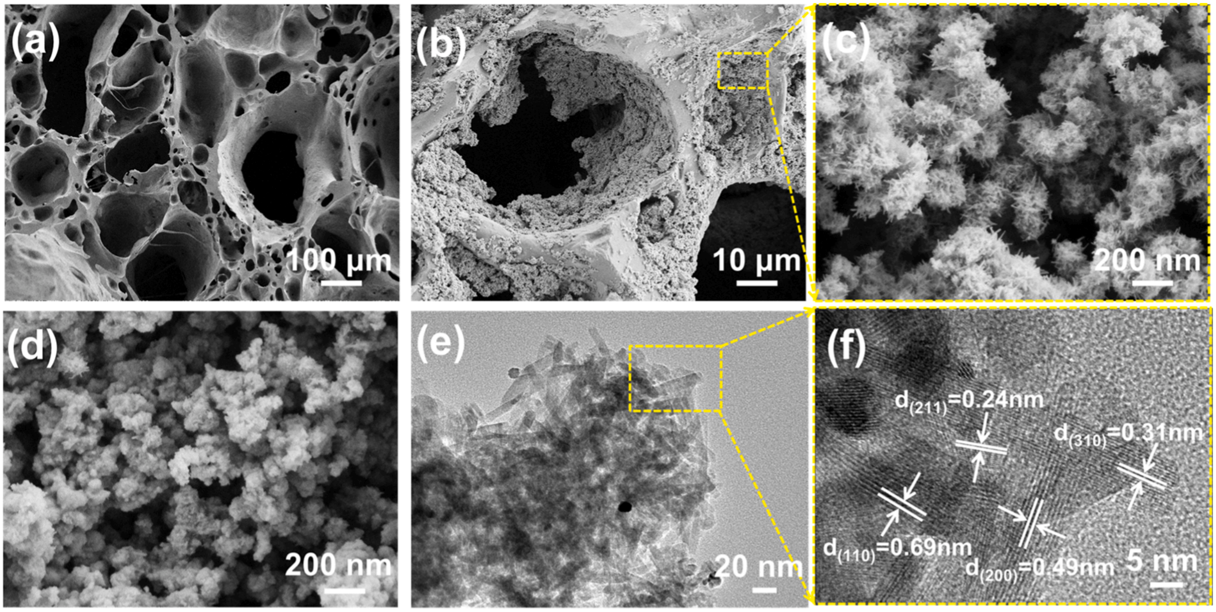

Fig. 3. FESEM images of (a) CF, (b, c) MnO_2/CF, and (d) MnO_2; HRTEM images of (e, f) MnO_2/CF.

CF support. Furthermore, the CF with special porous structure and oxygen-containing functional groups played as a favorable template, which provided abundant sites for the in-situ growth of MnO_2 nanoparticles and regulated their crystal structure and morphology [42]. The single MnO_2 sample exhibited nano-spherical particles (Fig. 3d). In contrast, the MnO_2 in MnO_2/CF composite showed spiny sphere-like nanoparticles (Fig. 3c). The hierarchical porous structure of CF could hinder the radial growth of MnO_2 nanofibers and promote the axial growth, thereby regulating the morphology of MnO_2.

HRTEM images (Fig. 3e) exhibit that the spiny sphere-like nanoparticles are formed by a large number of interwoven nanorods. Most of the reported α-MnO_2 catalysts presented a large-scale rod-like structure [38]. In contrast, this 3D structure formed by the interweaving of nanorods had a larger specific surface area, which exposed more active sites on the surface of the catalyst to promote catalytic activity. Furthermore, the MnO_2/CF sample showed clear crystal fringes of 0.24, 0.69, 0.49, and 0.31 nm on the (2 1 1), (1 1 0), (2 0 0), and (3 1 0) crystal planes, respectively (Fig. 3f).

3.1.5. XPS analysis

XPS analysis was applied to determine the elemental composition and surface chemical states of the catalyst, which can gain more insights into the influence of CF on the physicochemical properties of the catalyst. MnO_2 contained Mn and O element, and MnO_2/CF contained C, N, O, and Mn elements, which are confirmed by the full survey scan XPS spectra (Fig. S2a). As shown in Fig. 4a, the Mn element in MnO_2 and

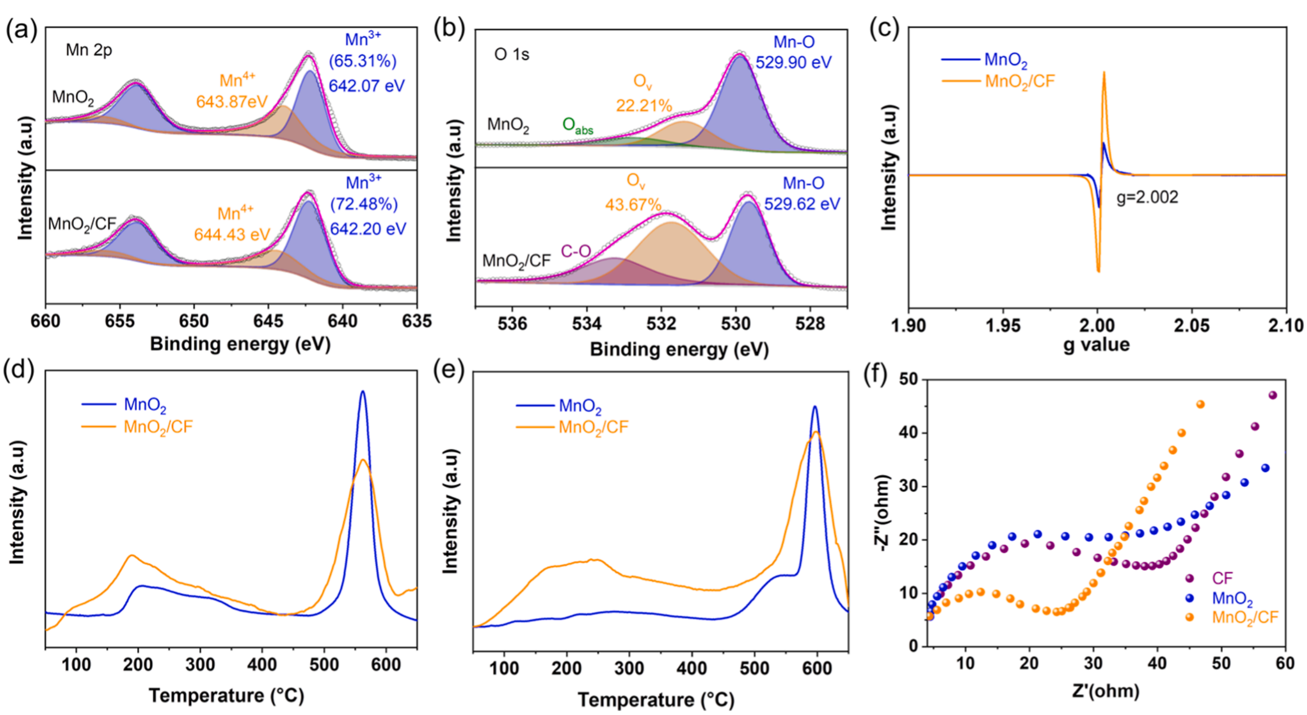

Fig. 4. High-resolution XPS spectra of (a) Mn 2p and (b) O 1s, (c) EPR spectra, (d) NH_3-TPD profile, (e) CO_2-TPD profile, and (f) EIS spectra of different samples.

MnO_2/CF existed in the form of Mn^{3+} and Mn^{4+}, and mainly the Mn^{3+}. Compared with the binding energies of Mn^{3+} (642.07 and 653.70 eV) and Mn^{4+} (643.87 and 656.12 eV) in single MnO_2, those of Mn^{3+} (642.20 and 653.77 eV) and Mn^{4+} (644.43 and 656.21 eV) in MnO_2/CF composite showed a positive shift, implying the electron transfer from MnO_2 to CF. In addition, the peak area ratio of Mn^{3+} (72.48%) in MnO_2/CF composite was higher than that (65.31%) in single MnO_2. The higher binding energy of Mn 2p and relative content of Mn^{3+} indicated more lattice defects in MnO_2/CF composite [43]. The formation of these defects may be due to the site occupancy effect of nitrogen atoms in the reaction interface of CF. Nitrogen atoms can interact with metal oxides to form interfacial stresses and modulate the surface electronic structure, resulting in an imbalance in charge distribution and the formation of oxygen defects [44]. O 1s XPS spectra (Fig. 4b) also manifested that the relative content of O_v in MnO_2/CF was significantly higher than that in MnO_2, revealing that MnO_2/CF could exhibit better catalytic oxidation activity [45–47]. Meanwhile, the binding energy of lattice oxygen (Mn–O) in MnO_2/CF decreased to 529.62 eV compared to that in MnO_2 (529.90 eV). This can be attributed to that the increased O_v concentration led to the enhanced electron density of lattice oxygen, thereby decreasing the binding energy of Mn–O in MnO_2/CF. N 1s spectrum of MnO_2/CF (Fig. S2b) presented that N could be deconvoluted into three peaks, corresponding to the nitrogen species of pyridine N (398.57 eV), pyrrole N (400.10 eV), and pyridine-N-oxide (402.48 eV). The lone pair electrons of pyridine N endow Lewis basic sites in carbon materials [48], so the introduction of CF could increase the Lewis basic sites of the MnO_2/CF catalyst. The basic sites on the surface of catalyst can promote the activation of hydroxyl and form the intermediate hemiacetal, which is conducive to the catalytic oxidation of HMF to FDCA. As shown in Fig. S2c, three peaks were fitted from C 1s spectrum of MnO_2/CF, including C–C (284.76 eV), C–O/C–N (286.16 eV), and C=O/C=N (288.77 eV). The binding energies of C–C, C–O/C–N, and C=O/C=N showed shift compared to their standard binding energies, indicating the existence of strong interfacial effects between MnO_2 and CF in MnO_2/CF composite.

3.2. Electrochemical and surface properties of the catalysts

EPR was applied to further test the presence of O_v, and the relative intensity of the EPR signal can directly reflect the O_v concentration. As presented in Fig. 4c, the spectra of all samples exhibited a typical signal at g = 2.002, representing the electrons trapped by O_v [49]. The signal intensity of MnO_2 was much weaker than that of MnO_2/CF, which further confirmed that the oxygen defects in CF and interfacial stress generated by nitrogen-doped carbon increased the O_v concentration on the surface of catalyst, corresponding to the XPS result. In the catalytic reaction system, the reactants can undergo further reactions by binding to the O_v and forming intermediates with oxygen on the catalyst. The O_v can also effectively regulate the electronic structure of the catalyst, enhance the electron enrichment effect, accelerate the adsorption and activation of O_2 on the catalyst, and change the charge transfer ability of the catalyst [16,50].

The surface acid-base properties of the catalysts were analyzed by NH_3-TPD and CO_2-TPD measurements, and the spectra are displayed in Fig. 4d and e. The amounts of total acid and basic sites determined based on integrated peak areas of the TPD profiles are summarized in Table 1. All samples presented the same acid-base type. In the NH_3-TPD spectra, the low-temperature desorption peak was attributed to the desorption of NH^{4+} bound to the Brønsted acid sites, and the high-temperature desorption peak was caused by the desorption of NH_3 from the Lewis acid ligand [51]. In the CO_2-TPD spectra, the low-temperature desorption peak was attributed to weak basic sites on the surface of catalyst, and the high-temperature desorption peak was attributed to the medium and strong basic sites [52]. The acid sites on the surface of catalyst play an important role in improving the yield of FDCA. The NH_3-TPD spectra of MnO_2 and MnO_2/CF catalysts presented obvious desorption peaks in both high temperature and low temperature regions, demonstrating that they had both Brønsted and Lewis acid sites. On the other hand, the surface basicity can improve the oxidation strength of the catalyst. The CO_2-TPD spectra of both catalysts exhibited sharp CO_2 desorption peaks in the high temperature region, indicating the strong basic sites on the surface of the catalysts. However, the MnO_2/CF catalyst had more basic sites (1.26 mmol g^{-1}), which could be contributed to higher oxidation activity. The introduction of CF significantly improved the acid and basic sites of the catalyst, which may be ascribed to that the oxygen-containing groups on the surface of CF could provide Brønsted acid sites and the nitrogen-containing species could provide Lewis base sites [53].

Table 1
Amounts of acid and basic sites obtained from NH_3-TPD and CO_2-TPD spectra.

Sample	Total acid sites (mmol g^{-1})	Total basic sites (mmol g^{-1})
MnO_2	1.55	0.46
MnO_2/CF	1.87	1.26

EIS was tested to explore the charge migration efficiency of the catalysts. As shown in Fig. 4f, all samples exhibit a semicircular impedance arc, and the smaller radius of the semi-arc reflects the lower resistance. As expected, MnO_2/CF composite had the smallest semi-arc, revealing the lowest resistance and best charge transfer. The in-situ growth of MnO_2 nanoparticles on CF formed intimate interface interaction with increased electron density, and the conductivity of carbon skeleton in CF contributed to the rapid transfer of electrons, thereby significantly improved the conductivity and electron transfer efficiency of MnO_2/CF composite. The high electrical conductivity and low charge transfer resistance can accelerate electron transfer in the catalyst, promote the oxidation/reduction cycle between Mn^{4+} and Mn^{3+}, and accelerate the regeneration of catalyst in the reaction process.

3.3. Adsorption capacity of the catalysts

Adsorption is a necessary step in the reaction, and the reaction can only occur if the reactant is captured on the active site. Therefore, adsorption and heterogeneous catalysis are closely related. In order to explore the adsorbability of catalyst for HMF substrate, the adsorption kinetics of three samples were tested, and the results are listed in Table S1. The 3D porous skeleton provided sufficient surface area for the adsorption of substrate and oxygen, enriching HMF and oxygen at the interface of CF and MnO_2, and the combination of efficient adsorption and oxidation could accelerate the oxidation of HMF. Meanwhile, the unique structure of α-MnO_2 contributed to excellent adsorption capacity [54]. The adsorption capacity of the catalyst can represent the capture ability of the catalyst for HMF substrate. The adsorption capacity of single CF and MnO_2 was 26.483 and 46.006 mg g^{-1}, respectively, while that of MnO_2/CF composite was 71.883 mg g^{-1}. The adsorption capacity of MnO_2/CF composite for HMF was much higher than that of single CF and MnO_2, indicating a synergistic effect between MnO_2 and CF, which could improve the catalytic performance of MnO_2/CF catalyst.

3.4. Catalytic performance of the catalysts

3.4.1. Effects of preparation concentration and different reaction conditions

The catalytic activity of the MnO_2/CF composites with various loading amount of MnO_2 prepared by varying the Mn^{2+} concentration was investigated to confirm the optimal loading amount of MnO_2. As shown in Fig. S3, the yield of FDCA showed an upward trend as the increase of the Mn^{2+} concentration in the solution, but it became slightly decreased after 1.80 M. Therefore, 1.80 M was chosen as the optimal preparation concentration of catalyst to further study the effects of other reaction parameters. The ICP result showed that the percentage of MnO_2 in the MnO_2/CF catalyst prepared from the Mn^{2+} concentration of 1.80 M was 9.84%.

The time course of the catalytic oxidation of HMF to FDCA over MnO_2 and MnO_2/CF catalysts were recorded under the same conditions (Fig. 5). Evidently, MnO_2/CF composite exhibited better catalytic performance. The two catalysts achieved complete conversion of HMF, but the selectivity of products was significantly different. For MnO_2 catalyst, the yield of FDCA increased with the increase of time, and reached the best value of 65.3% at 3 h. With the continuous increase of reaction time, the yield of FDCA did not increase but decreased slightly, indicating that the reaction reached the bottleneck. For MnO_2/CF catalyst, the yield of FDCA reached the best value of 97.0% at 2 h, which far exceeded that of the MnO_2 catalyst. In addition, no DFF was detected during the reaction, and only a small amount of HMFCA was found in the initial stage of the reaction (<1.5 h), which may be that the reaction proceeded through a pathway involving the preferential oxidation of aldehyde groups. The catalytic oxidation of HMF to FDCA usually includes two reaction routes (Fig. 6). For the reaction system in this study, HMFCA intermediate was generated first instead of DFF. It was worth noting that the conversion rate of HMF was>99% at 0.5 h, but poor carbon balance was obtained, which may be related to the strong adsorption of HMF on the catalyst.

The effect of reaction temperature on the catalytic oxidation of HMF over MnO_2/CF catalyst was examined at 0.3 MPa for 2 h (Fig. S4). In the low temperature region (<90 °C), the main reaction product was FFCA, and FFCA was gradually transformed into FDCA with the increase of temperature. Accordingly, temperature was an important factor for FFCA to be transformed into FDCA. In the high temperature region (>100 °C), the yield of FDCA decreased gradually, which might be because HMF was degraded to humic acid.

Subsequently, the catalytic behavior of MnO_2/CF was investigated at different oxygen pressures, and the results are shown in Fig. S5. The yield of FDCA increased significantly with rising oxygen pressure, and obtained the maximum value at 0.3 MPa. Oxygen pressure affects electron transfer and regeneration of catalyst during the reaction. The role of oxygen was explored by conducting the catalytic reaction in the absence of oxygen (1 MPa N_2). The conversion rate of HMF could still reach 97.6% in the absence of oxygen, but the yield of oxidation product was very low. Interestingly, a considerable yield of HMFCA was obtained, revealing that the conversion of HMF to HMFCA can also proceed without the participation of oxygen.

Catalyst dosage has a significant effect on the degree of progress of the reaction. As shown in Fig. S6, both HMF conversion and FDCA yield increased with increasing the dosage of MnO_2/CF catalyst. Especially, catalyst dosage remarkably influenced the yield of FDCA, and HMF was almost completely converted to FDCA with 0.4 g of MnO_2/CF. It is noteworthy that a HMF conversion rate of 34.2% could be achieved without the addition of catalyst, but there were almost no oxidation products. In this case, HMF was degraded and almost no oxidation reaction occurred, indicating that catalyst was crucial for the oxidation reaction of HMF.

The addition of a base compound can promote the formation of alcohols and the activation of C–H bonds [55]. The effect of $NaHCO_3$ dosage on the selective oxidation of HMF to FDCA over MnO_2/CF catalyst was evaluated. Without $NaHCO_3$, HMF conversion rate was 85.4%, and FFCA yield was 42.3% (Fig. S7). As observed, HMF could be oxidated in the absence of base additive, attributed to that the basic sites of the catalyst itself could act like an external base to promote the formation of FFCA from HMF. When the addition amount of $NaHCO_3$ was 0.5 (equiv.) or less, FFCA was the main product. With the increase of $NaHCO_3$ dosage, FFCA gradually transformed to FDCA. As a result, the addition of external base promoted the conversion of FFCA to FDCA.

3.4.2. Active components of the MnO_2/CF catalyst

The catalytic activity of CF was investigated under the optimal reaction conditions (2 h, 0.3 MPa, 100 °C), and HMF conversion was only 22.9%, with FFCA yield of 0.64% and no formation of FDCA. It could be concluded that the active sites of the MnO_2/CF catalyst were mainly MnO_2, and the role of CF was to serve as a support and provided a favorable template for the growth of MnO_2 with unique characteristics. The synergistic effect between the support and the active components improved the properties of the catalyst, especially the enhanced O_v concentration and charge transfer efficiency, contributing to the excellent catalytic activity of MnO_2/CF composite.

3.4.3. Recyclability of the MnO_2/CF catalyst

Five cycle experiments were carried out under optimal conditions to demonstrate the reusability of the MnO_2/CF catalyst (Fig. 7a). In the first cycle, the HMF conversion and FDCA yield were 99.8% and 97.0%, respectively. After five cycles, the HMF conversion and FDCA yield slightly decreased to 96.6% and 90.2%, verifying good reusability of the as-prepared MnO_2/CF catalyst. The MnO_2/CF catalyst after used for five cycles was analyzed by XRD and XPS to further confirm the structural stability. As illustrated in Fig. 7b, the diffraction peaks in the XRD patterns of fresh and used MnO_2/CF catalysts were almost no differences, revealing that the crystal structure of MnO_2 was stable. The XPS full survey scan spectra (Fig. 7c) and high-resolution Mn 2p spectra (Fig. S8) of the catalyst before and after reaction were no noticeable change, demonstrating that the surface elemental composition and the valence composition of Mn element in the MnO_2/CF catalyst were stable. The reaction solution was further characterized by ICP, and the Mn content in the solution was almost negligible, indicating that the MnO_2/CF catalyst did not experience noticeable leaching of active metals during the reaction. Therefore, the MnO_2/CF catalyst exhibited good stability and reusability for catalytic oxidation of HMF. Especially, the CF with block structure led to easy separation of MnO_2/CF catalyst from the

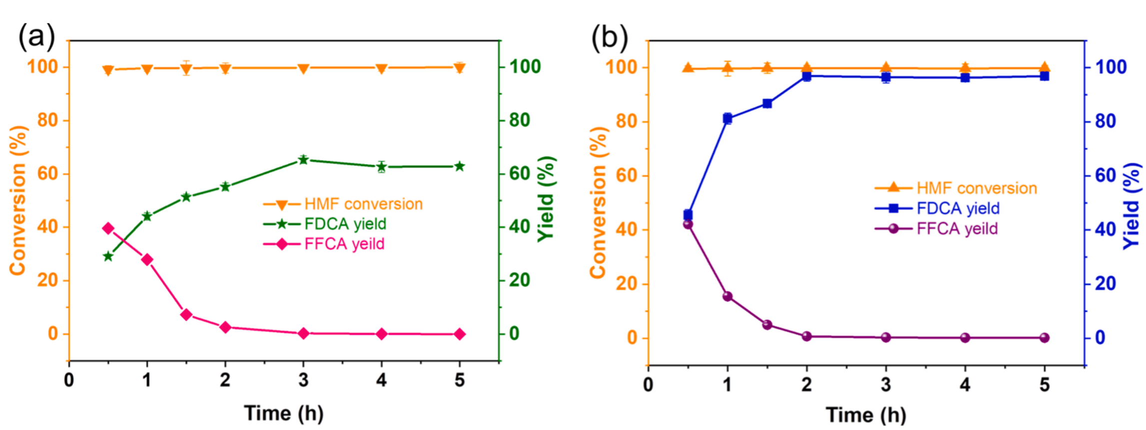

Fig. 5. Time-conversion diagram of the oxidation of HMF to FDCA over (a) MnO_2 catalyst and (b) MnO_2/CF catalyst. Reaction conditions: HMF (0.25 mmol), MnO_2 catalyst (40 mg) or MnO_2/CF catalyst (0.4 g, MnO_2 content of 40 mg), H_2O (5 mL), O_2 (0.3 MPa), 100 °C, $NaHCO_3$/HMF = 2.

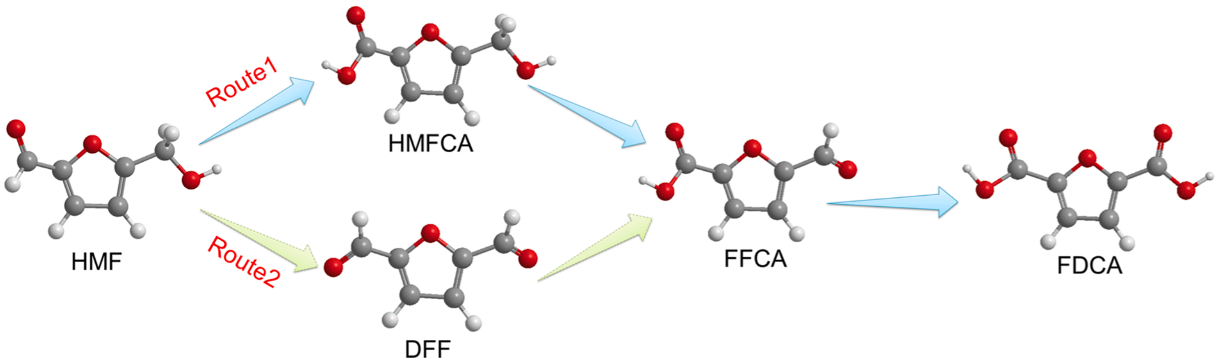

Fig. 6. Reaction pathway of aerobic oxidation of HMF to FDCA.

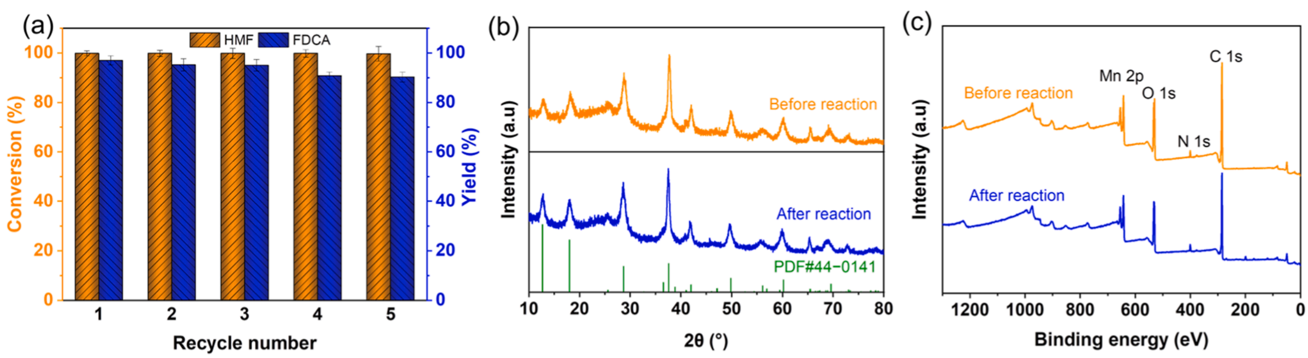

Fig. 7. (a) Reusability of the MnO_2/CF catalyst. Reaction conditions: HMF (0.25 mmol), catalyst (0.4 g), H_2O (5 mL), O_2 (0.3 MPa), 100 °C, 2 h, $NaHCO_3$/HMF = 2; (b) XRD patterns of the MnO_2/CF catalyst before and after reaction; (c) full survey scan XPS spectra of the MnO_2/CF catalyst before and after reaction.

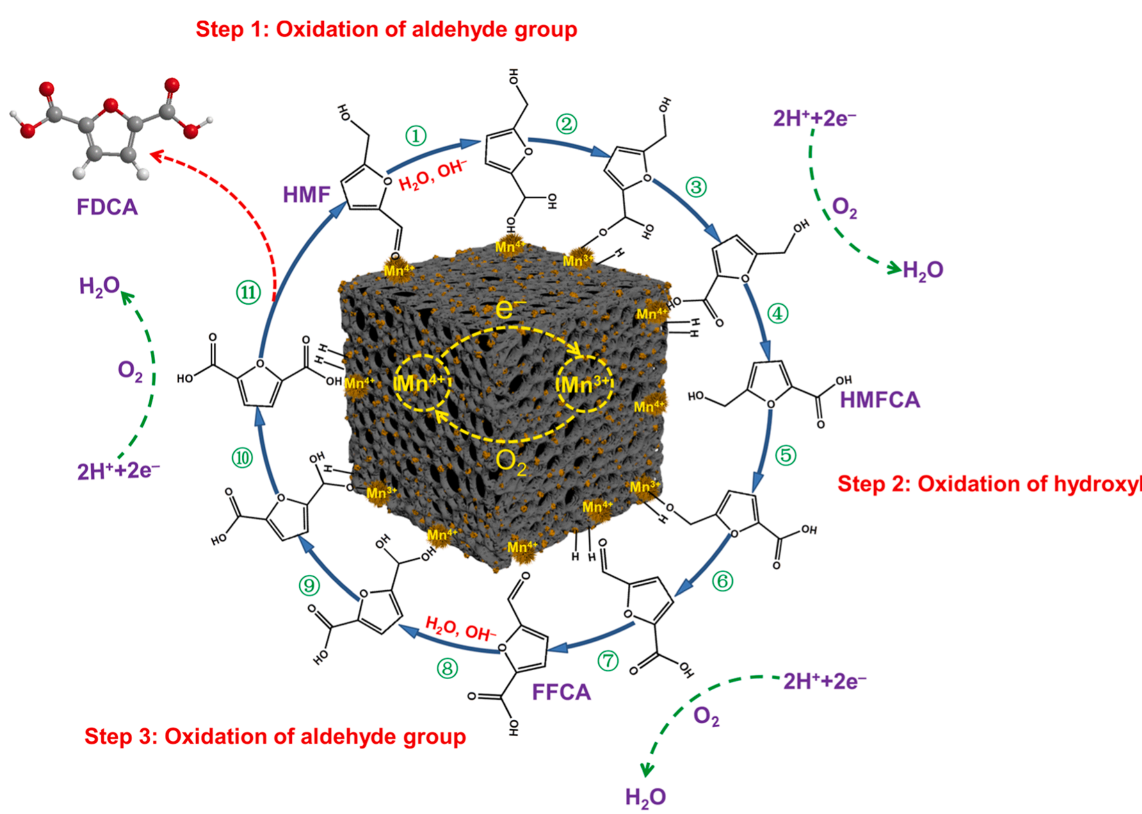

Fig. 8. Possible reaction mechanism for the aerobic oxidation of HMF to FDCA over MnO_2/CF catalyst.

reaction system, and the CF support with high mechanical strength could prevent the breakage of catalyst and facilitate recycling.

3.5. Catalytic reaction mechanism

According to the results in this study and the mechanisms reported in previous literatures [56], the possible reaction mechanism for the oxidation of HMF to FDCA over MnO_2/CF catalyst was proposed, as shown in Fig. 8. The reaction process is divided into three stages. In the first stage, the aldehyde group of HMF is oxidized to carboxyl group to generate HMFCA; in the second stage, the hydroxyl group of HMFCA is oxidized to aldehyde group to generate FFCA; in the third stage, the aldehyde group of FFCA is oxidized to carboxyl group to generate FDCA. In the alkaline environment, the surface acidic sites and O_v of the catalyst simultaneously promote the adsorption of aldehyde groups on the surface of catalyst. Therefore, the reaction pathway follows the preferential oxidation of aldehyde groups, which is similar to the oxidation pathway of HMF over noble metal-based catalysts. OH– attacks the aldehyde group of HMF, and the hydration reaction occurs under the promotion of the basic sites of the catalyst to split into hemiacetal. Subsequently, the hydroxyl group of hemiacetal is adsorbed on the Mn^{4+} of the catalyst, and the electrons are transferred to the catalyst. As the formation of Mn^{3+}-alcohol oxygen intermediate, the dehydrogenation is continued to generate HMFCA. The oxygen adsorbed on the catalyst is activated to oxidize Mn^{3+} to Mn^{4+}, completing the regeneration of the catalyst and takes two protons and electrons to convert into water. The second stage is similar to the dehydrogenation of hemiacetal in the first stage. The hydroxyl groups of HMFCA are activated at the basic sites of the catalyst, and electrons are transferred to the Mn^{4+} of the catalyst to form a Mn^{3+}-aldehyde intermediate, which is oxidatively dehydrogenated to form FFCA. The steps of the third stage are similar to those of the first stage, and the target product FDCA is finally obtained. During the reaction, electrons are first transferred to CF, which are quickly captured by Mn^{4+} on the surface and then proceed to the next reaction step. The rapid progress of this process depends on the high electrical conductivity of the catalyst and the formation of intimate interface interaction.

4. Conclusions

In summary, a novel and facile method was developed for in-situ growth of spiny sphere-like MnO_2 nanoparticles on 3D hierarchical porous CF to prepare blocky MnO_2/CF catalyst, which exhibited favorable catalytic performance for the oxidation of HMF to FDCA. Comparative investigation of single MnO_2, CF, and MnO_2/CF composite indicated that the CF with oxygen-containing groups provided abundant sites for in-situ growth of MnO_2 nanoparticles and also regulated their crystal structure and morphology. The introduction of CF for supporting MnO_2 led to enhanced specific surface area, O_v concentration, surface acid-base sites, and charge transfer efficiency of MnO_2/CF composite, thereby promoting the adsorption and activation of HMF and O_2 on the catalyst, which significantly improved the catalytic performance of the MnO_2/CF catalyst. Under the mild reaction conditions (100 °C, 0.3 MPa O_2, 2 h), HMF conversion of 99.8% and FDCA yield of 97.0% were obtained over MnO_2/CF catalyst. After five cycles, the catalytic activity and structure of the catalyst almost did not change, verifying that MnO_2/CF composite exhibited good stability and reusability. In this contribution, a new strategy is proposed to develop efficient, stable, economical, and environmentally friendly blocky manganese-based catalysts.

CRediT authorship contribution statement

Min Jiang: Conceptualization, Methodology, Software, Investigation, Validation, Writing – original draft. **Furui Hu:** Conceptualization, Data curation, Investigation. **Guifen Feng:** Data curation, Methodology, Investigation. **Hongguang Zhang:** Methodology, Software, Investigation. **Huayu Hu:** Conceptualization, Funding acquisition, Methodology, Supervision, Project administration, Writing – review & editing. **Tao Gan:** Visualization, Investigation. **Zuqiang Huang:** Supervision, Resources. **Yanjuan Zhang:** Conceptualization, Funding acquisition, Methodology, Supervision, Writing – review & editing.

Declaration of Competing Interest

The authors declare that they have no known competing financial interests or personal relationships that could have appeared to influence the work reported in this paper.

Acknowledgements

This research was supported by National Natural Science Foundation of China (No. 22008041) and Guangxi Natural Science Foundation, China (Nos. 2019GXNSFDA245020 and 2020GXNSFGA297001).

Appendix A. Supplementary material

Supplementary data to this article can be found online at https://doi.org/10.1016/j.apsusc.2022.153849.

References

[1] X. Chen, N. Yan, A brief overview of renewable plastics, Mater. Today Sustain. 7–8 (2020), 100031.
[2] Z. Zhang, G.W. Huber, Catalytic oxidation of carbohydrates into organic acids and furan chemicals, Chem. Soc. Rev. 47 (4) (2018) 1351–1390.
[3] J. Chheda, G. Huber, J. Dumesic, Liquid-phase catalytic processing of biomass-derived oxygenated hydrocarbons to fuels and chemicals, Angew. Chem. Int. Ed. 46 (38) (2007) 7164–7183.
[4] M. Li, F. Xu, H. Li, Y. Wang, Nitrogen-doped porous carbon materials: promising catalysts or catalyst supports for heterogeneous hydrogenation and oxidation, Catal. Sci. Technol. 6 (2016) 367–3693.
[5] Y. Román-Leshkov, J.N. Chheda, J.A. Dumesic, Phase modifiers promote efficient production of hydroxymethylfurfural from fructose, Science 312 (5782) (2006) 1933–1937.
[6] M. Sajid, X. Zhao, D. Liu, Production of 2,5-furandicarboxylic acid (FDCA) from 5-hydroxymethylfurfural (HMF): recent progress focusing on the chemical-catalytic routes, Green Chem. 20 (2018) 5427–5453.
[7] J. Lan, J. Lin, Z. Chen, G. Yin, Transformation of 5-hydroxymethylfurfural (HMF) to maleic anhydride by aerobic oxidation with heteropolyacid catalysts, ACS Catal. 5 (4) (2015) 2035–2041.
[8] Z. Zhang, K. Deng, Recent advances in the catalytic synthesis of 2,5-furandicarboxylic acid and its derivatives, ACS Catal. 5 (11) (2015) 6529–6544.
[9] K. Hwang, W. Jeon, S.Y. Lee, M. Kim, Y. Park, Sustainable bioplastics: recent progress in the production of bio-building blocks for the bio-based next-generation polymer PEF, Chem. Eng. J. 390 (2020), 124636.
[10] S. Wang, Z. Zhang, B. Liu, Catalytic conversion of fructose and 5-hydroxymethylfurfural into 2,5-furandicarboxylic acid over a recyclable fe_3o_4-coo_x magnetite nanocatalyst, ACS Sustainable Chem. Eng. 3 (3) (2015) 406–412.
[11] X. Zuo, P. Venkitasubramanian, D.H. Busch, B. Subramaniam, Optimization of Co/Mn/Br-catalyzed oxidation of 5-hydroxymethylfurfural to enhance 2,5-furandicarboxylic acid yield and minimize substrate burning, ACS Sustainable Chem. Eng. 4 (7) (2016) 3659–3668.
[12] Q. Li, H. Wang, Z. Tian, Y. Weng, C. Wang, J. Ma, C. Zhu, W. Li, Q. Liu, L. Ma, Selective oxidation of 5-hydroxymethylfurfural to 2,5-furandicarboxylic acid over Au/CeO_2 catalysts: the morphology effect of CeO_2, Catal. Sci. Technol. 9 (7) (2019) 1570–1580.
[13] B. Donoeva, N. Masoud, P.E. de Jongh, Carbon support surface effects in the gold-catalyzed oxidation of 5-hydroxymethylfurfural, ACS Catal. 7 (7) (2017) 4581–4591.
[14] W. Guan, Y. Zhang, Y. Chen, J. Wu, Y. Cao, Y. Wei, P. Huo, Hierarchical porous bowl-like nitrogen-doped carbon supported bimetallic AuPd nanoparticles as nanoreactors for high efficient catalytic oxidation of HMF to FDCA, J. Catal. 396 (2021) 40–53.
[15] Y. Liao, V.C. Nguyen, N. Ishiguro, A.P. Young, C. Tsung, K.C.W. Wu, Engineering a homogeneous alloy-oxide interface derived from metal-organic frameworks for selective oxidation of 5-hydroxymethylfurfural to 2,5-furandicarboxylic acid, Appl. Catal. B Environ. 270 (2020), 118805.
[16] A.I.M. Rabee, S.D. Le, K. Higashimine, S. Nishimura, Aerobic oxidation of 5-hydroxymethylfurfural into 2,5-furandicarboxylic acid over gold stabilized on zirconia-based supports, ACS Sustainable Chem. Eng. 8 (18) (2020) 7150–7161.
[17] K.T.V. Rao, J.L. Rogers, S. Souzanchi, A.M.B.R.D. Luana, Inexpensive but highly efficient Co-Mn mixed oxide catalysts prepared by simple solid-state mixing for selective oxidation of 5-hydroxymethylfurfural to 2,5-furandicarboxylic acid, ChemSusChem 13 (2018) 287–288.

[18] X. Han, C. Li, X. Liu, Q. Xia, Y. Wang, Selective oxidation of 5-hydroxymethylfurfural to 2,5-furandicarboxylic acid over MnO_x-CeO_2 composite catalysts, Green Chem. 19 (4) (2017) 996–1004.

[19] T. Hu, High-efficient aerobic oxidation of biomass-derived 5-hydroxymethylfurfural to 2,5-furandicarboxylic acid over holey 2D Mn_2O_3 nanoflakes from a Mn-based MOF, J. Subst. Abus. Treat. 13 (2019) 287–288.

[20] E. Hayashi, T. Komanoya, K. Kamata, M. Hara, Heterogeneously-catalyzed aerobic oxidation of 5-hydroxymethylfurfural to 2,5-furandicarboxylic acid with manganese dioxide, ChemSusChem 13 (2016) 287–288.

[21] F. Neaţu, R.S. Marin, M. Florea, N. Petrea, O.D. Pavel, V.I. Pârvulescu, Selective oxidation of 5-hydroxymethyl furfural over non-precious metal heterogeneous catalysts, Appl. Catal. B Environ. 180 (2016) 751–757.

[22] T. Gao, Y. Yin, G. Zhu, Q. Cao, W. Fang, Co_3O_4 NPs decorated Mn-Co-O solid solution as highly selective catalyst for aerobic base-free oxidation of 5-HMF to 2,5-FDCA in water, Catal. Today 355 (2020) 252–262.

[23] J. Lai, F. Cheng, S. Zhou, S. Wen, D. Guo, W. Zhao, X. Liu, D. Yin, Base-free oxidation of 5-hydroxymethylfurfural to 2, 5-furan dicarboxylic acid over nitrogen-containing polymers supported Cu-doped MnO_2 nanowires, Appl. Surf. Sci. 565 (2021), 150479.

[24] H. Liu, W. Jia, X. Yu, X. Tang, X. Zeng, Y. Sun, T. Lei, H. Fang, T. Li, L. Lin, Vitamin C-assisted synthesized Mn–Co oxides with improved oxygen vacancy concentration: boosting lattice oxygen activity for the air-oxidation of 5-(hydroxymethyl)furfural, ACS Catal. 11 (2021) 7828–7844.

[25] H. Zhou, H. Xu, Y. Liu, Aerobic oxidation of 5-hydroxymethylfurfural to 2,5-furandicarboxylic acid over Co/Mn-lignin coordination complexes-derived catalysts, Appl. Catal. B Environ. 244 (2019) 965–973.

[26] Y. Wei, Y. Zhang, Y. Chen, F. Wang, Y. Cao, W. Guan, X. Li, Crystal faces-tailored oxygen vacancy in Au/CeO_2 catalysts for efficient oxidation of HMF to FDCA, ChemSusChem 14 (2021) 1–12.

[27] Y. Wang, K. Yu, D. Lei, W. Si, Y. Feng, L.-L. Lou, S. Liu, Basicity-tuned hydrotalcite-supported Pd catalysts for aerobic oxidation of 5-hydroxymethyl-2-furfural under mild conditions, ACS Sustainable Chem. Eng. 4 (9) (2016) 4752–4761.

[28] D. Yan, J. Xin, Q. Zhao, K. Gao, X. Lu, Fe–Zr–O catalyzed base-free aerobic oxidation of 5-HMF to 2,5-FDCA as a bio-based polyester monomer, Catal. Sci. Technol. 8 (2018) 164.

[29] Y. Li, Z. Xu, D. Wang, J. Zhao, H. Zhang, Snowflake-like core-shell α-MnO_2@δ-MnO_2 for high performance asymmetric supercapacitor, Electrochim. Acta 251 (2017) 344–354.

[30] J. Huang, S. Zhong, Y. Dai, C.-C. Liu, H. Zhang, Effect of MnO_2 phase structure on the oxidative reactivity toward bisphenol A degradation, Environ. Sci. Technol. 52 (19) (2018) 11309–11318.

[31] J. Ma, C. Wang, H. He, Transition metal doped cryptomelane-type manganese oxide catalysts for ozone decomposition, Appl. Catal. B Environ. 201 (2017) 503–510.

[32] L. Miao, J. Wang, P. Zhang, Review on manganese dioxide for catalytic oxidation of airborne formaldehyde, Appl. Surf. Sci. 466 (2019) 441–453.

[33] H. Wang, X. Cai, Y. Zhang, T. Zhang, M. Chen, H. Hu, Z. Huang, J. Liang, Y. Qin, Double-template-regulated bionic mineralization for the preparation of flower-like BiOBr/carbon foam/PVP composite with enhanced stability and visible-light-driven catalytic activity, Appl. Surf. Sci. 555 (2021), 149708.

[34] Y. Zhang, M. Zhao, H. Wang, H. Hu, R. Liu, Z. Huang, C. Chen, D. Chen, Z. Feng, Damaged starch derived carbon foam-supported heteropolyacid for catalytic conversion of cellulose: improved catalytic performance and efficient reusability, Bioresource Technol. 288 (2019), 121532.

[35] Y. Yang, D. Deng, S. Zhang, Q. Meng, Z. Li, Z. Wang, H. Sha, R. Faller, Z. Bian, X. Zou, G. Zhu, Y. Yuan, Porous organic frameworks featured by distinct confining fields for the selective hydrogenation of biomass-derived ketones, Adv. Mater. 32 (2020) 1908243.

[36] G. Zhu, W. Zhu, Y. Lou, J. Ma, W. Yao, R. Zong, Y. Zhu, Encapsulate α-MnO_2 nanofiber within graphene layer to tune surface electronic structure for efficient ozone decomposition, Nat. Commun. 12 (2021) 4152–4161.

[37] H. Yu, K.-A. Kim, M.J. Kang, S.Y. Hwang, H.G. Cha, Carbon support with tunable porosity prepared by carbonizing chitosan for catalytic oxidation of 5-hydroxylmethylfurfural, ACS Sustainable Chem. Eng. 7 (4) (2019) 3742–3748.

[38] E. Hayashi, Y. Yamaguchi, K. Kamata, N. Tsunoda, Y.u. Kumagai, F. Oba, M. Hara, Effect of MnO_2 crystal structure on aerobic oxidation of 5-hydroxymethylfurfural to 2,5-furandicarboxylic acid, J. Am. Chem. Soc. 141 (2) (2019) 890–900.

[39] X. Qian, M. Ren, D. Yue, Y. Zhu, Y. Han, Z. Bian, Y. Zhao, Mesoporous TiO_2 films coated on carbon foam based on waste polyurethane for enhanced photocatalytic oxidation of VOCs, Appl. Catal. B Environ. 212 (2017) 1–6.

[40] Y. Boyjoo, G. Rochard, J.-M. Giraudon, J. Liu, J.-F. Lamonier, Mesoporous MnO_2 hollow spheres for enhanced catalytic oxidation of formaldehyde, Sustain. Mater. Technol. 20 (2019) e00091.

[41] J. Zhou, L. Qin, W. Xiao, C. Zeng, N. Li, T. Lv, H. Zhu, Oriented growth of layered-MnO_2 nanosheets over α-MnO_2 nanotubes for enhanced room-temperature HCHO oxidation, Appl. Catal. B Environ. 207 (2017) 233–243.

[42] S. Chen, J. Zhu, X. Wu, Q. Han, X. Wang, Graphene oxide−MnO_2 nanocomposites for supercapacitors, ACS Nano 4 (5) (2010) 2822–2830.

[43] S.C. Kim, W.G. Shim, Catalytic combustion of VOCs over a series of manganese oxide catalysts, Appl. Catal. B Environ. 98 (3-4) (2010) 180–185.

[44] J. Zhong, Y. Feng, B. Yang, Q. Xiong, G.-G. Ying, Accelerated degradation of sulfadiazine by nitrogen-doped magnetic biochar-activated persulfate: role of oxygen vacancy, Sep. Purif. Technol. 289 (2022) 120735.

[45] K.-Y. Lin, W.-D. Oh, M.-W. Zheng, E. Kwon, J. Lee, J.-Y. Lin, X. Duan, F. Ghanbari, Aerobic oxidation of 5-hydroxymethylfurfural into 2,5-diformylfuran using manganese dioxide with different crystal structures: a comparative study, J. Colloid Interface Sci. 592 (2021) 416–429.

[46] R. Yang, Z. Guo, L. Cai, R. Zhu, Y. Fan, Y. Zhang, W.Z.X.Z. Pingping Han, A.Z. Z. Chak Keung Chan, Investigation into the phase-activity relationship of MnO_2 nanomaterials toward ozone-assisted catalytic oxidation of toluene, Small 17 (2021) 1–11.

[47] C.V. Nguyen, Y.-T. Liao, T.-C. Kang, J.E. Chen, T. Yoshikawa, Y. Nakasaka, T. Masuda, K.-W. Wu, A metal-free, high nitrogen-doped nanoporous graphitic carbon catalyst for an effective aerobic HMF-to-FDCA conversion, Green Chem. 18 (22) (2016) 5957–5961.

[48] Y. Cao, S. Mao, M. Li, Y. Chen, Y. Wang, Metal/porous carbon composites for heterogeneous catalysis: old catalysts with improved performance promoted by N-doping, ACS Catal. 7 (2017) 8090–8112.

[49] Y. Lu, T. Liu, C.L. Dong, C. Yang, L. Zhou, Y.C. Huang, Y. Li, B. Zhou, Y. Zou, S. Wang, Tailoring competitive adsorption sites by oxygen-vacancy on cobalt oxides to enhance the electrooxidation of biomass, Adv. Mater. 34 (2022) 2107185.

[50] Z. Zhang, S. Li, B. Zhao, X. Zhang, X. Wang, Z. Wen, S. Ji, J. Sun, Joint influence of nitrogen doping and oxygen vacancy on manganese dioxide as a high-capacity cathode for zinc-ion batteries, J. Phys. Chem. C 125 (37) (2021) 20195–20203.

[51] D.K. Mishra, H.J. Lee, J. Kim, H.-S. Lee, J.K. Cho, Y.-W. Suh, Y. Yi, Y.J. Kim, $MnCo_2O_4$ spinel supported ruthenium catalyst for air-oxidation of HMF to FDCA under aqueous phase and base-free conditions, Green Chem. 19 (7) (2017) 1619–1623.

[52] F. Neaţu, N. Petrea, R. Petre, V. Somoghi, M. Florea, V.I. Parvulescu, Oxidation of 5-hydroxymethyl furfural to 2,5-diformylfuran in aqueous media over heterogeneous manganese based catalysts, Catal. Today 278 (2016) 66–73.

[53] K.T.V. Rao, Y. Hu, Z. Yuan, Y. Zhang, C.C. Xu, Nitrogen-doped carbon: a metal-free catalyst for selective oxidation of crude 5-hydroxymethylfurfural obtained from high fructose corn syrup (HFCS-90) to 2,5-furandicarboxylic acid (FDCA), Chem. Eng. J. 404 (2021), 127063.

[54] G. Zhu, J. Zhu, W. Jiang, Z. Zhang, J. Wang, Y. Zhu, Q. Zhang, Surface oxygen vacancy induced α-MnO_2 nanofiber for highly efficient ozone elimination, Appl. Catal. B Environ. 209 (2017) 729–737.

[55] X. Liu, M. Zhang, Z. Li, CoO_x-MC (MC = mesoporous carbon) for highly efficient oxidation of 5-hydroxymethylfurfural (5-HMF) to 2,5-furandicarboxylic acid (FDCA), ACS Sustainable Chem. Eng. 8 (12) (2020) 4801–4808.

[56] X. Kong, Y. Zhu, Z. Fang, J.A. Kozinski, I.S. Butler, L. Xu, H.e. Song, X. Wei, Catalytic conversion of 5-hydroxymethylfurfural to some value-added derivatives, Green Chem. 20 (16) (2018) 3657–3682.